Dosimetry and Monte Carlo modelling of the Papillon plus contact X-ray brachytherapy device

Peer-reviewed author version

COLSON, Dries; YALVAC, Burak; Weterings, Jan; Verrijssen, An-Sofie; van Haaren, Paul; Bellezzo, Murillo; Berbee, Maaike; Van Limbergen, Evert J.; Croce, Olivier; Verhaegen, Frank & RENIERS, Brigitte (2024) Dosimetry and Monte Carlo modelling of the Papillon plus contact X-ray brachytherapy device. In: Brachytherapy, 23 (5) , p. 535 -548.

DOI: 10.1016/j.brachy.2024.06.003
Handle: http://hdl.handle.net/1942/44273

Dosimetry and Monte Carlo Modelling of the Papillon+ Contact X-ray Brachytherapy Device

Dries Colson[1], Burak Yalvac[1], Jan Weterings[2], An-Sofie Verrijssen[2], Paul van Haaren[2], Murillo Bellezzo[3], Maaike Berbée[3], Evert J. Van Limbergen[3], Olivier Croce[4], Frank Verhaegen[3], Brigitte Reniers[1]

[1] *Hasselt University, Faculty of Engineering Technology - Nuclear Technological Centre (NuTeC), Hasselt, Belgium*

[2] *Catharina Hospital, Department of Radiation Oncology, Eindhoven, The Netherlands*

[3] *Department of Radiation Oncology (MAASTRO), GROW Research Institute for Oncology and Reproduction, Maastricht University Medical Center, the Netherlands*

[4] *Institute for Research on Cancer and Aging of Nice (IRCAN), CNRS, INSERM, Université Côte d'Azur, Nice, France*

*Corresponding author: brigitte.reniers@uhasselt.be, Hasselt University, Martelarenlaan 42, 3500 Hasselt, Belgium)

Abstract

Purpose: This study aimed to develop and validate a Monte Carlo (MC) model for the Papillon+ contact x-ray brachytherapy (CXB) device, producing 50 kilovolt (kV) x-rays, specifically focusing on its application with a 25 mm diameter rectal applicator for contact therapy.

Material and methods: The validation process involved depth dose and transverse dose profile measurements using EBT3 gafchromic films positioned in a Plastic Water Low Energy Range phantom. The half-value layer (HVL) was further measured and derived from the simulated x-ray spectra.

Results: Excellent agreement within ± 2 % was achieved between the measured and simulated on-axis depth dose curves for the 25 mm rectal applicator. Transverse dose profile measurements showed a high level of agreement between the simulation and measurements, on average 3.1 % in contact with the applicator at the surface of the phantom and on average 1.7 % at 10 mm depth. A close agreement within 5.5 % was noticed concerning the HVL between the measurement and simulation. The simulated gamma spectra and 2D-dose distribution demonstrated a soft x-ray energy spectrum and a uniform dose distribution in contact with the applicator.

Conclusions: An MC model was successfully developed for the Papillon+ eBT device with a 25 mm diameter rectal applicator. The validated model, with its demonstrated accuracy in depth dose and transverse dose profile simulations, is a valuable tool for quality assurance and patient safety and, in a later phase, may be used for treatment planning, dose calculations and tissue inhomogeneity corrections.

Keywords

Monte Carlo modelling

Contact x-ray brachytherapy

Papillon treatment

Rectal cancer

Introduction

In recent years, contact x-ray brachytherapy (CXB) has emerged as a promising modality that uses low-energy x-rays for the localised contact treatment of various superficial malignancies, including benign lesions and malignant tumours, offering a precise and targeted approach to deliver therapeutic radiation [1] [2] [3] [4]. Seven different types of eBT systems are currently available specifically designed for the contact treatment with low-energy x-rays of, for example, rectal tumours, skin lesions or breast tumours, including Intrabeam® (Carl Zeiss, Oberkochen, Germany), Xoft® Axxent® (Elekta, Stockholm, Sweden), Papillon+™ (Ariane™ Medical Systems, Alfreton, United Kingdom), Radiant™ Aura and Xstrahl devices (Xstrahl Inc., Suwanee, Georgia, USA), Esteya® (Elekta, Stockholm, Sweden) and SRT-100+™ (Sensus Healthcare, Boca Raton, Florida, USA). Contact x-ray brachytherapy gains momentum in clinical applications, as illustrated, e.g. by the OPERA trial comparing in the case of a rectum tumour a radiotherapeutic boost by CXB with a boost by external beam radiotherapy combined with external beam chemoradiotherapy for early rectal adenocarcinoma. It was concluded that the 3-year organ preservation rate significantly improved by 20% with chemoradiotherapy and a CXB boost. In patients with tumours smaller than 3 cm who received initial treatment with CXB, the success rate was almost 40 % [5]. Following the considerable success of the OPERA trial, adoption rates are expected to increase significantly, and therefore, the importance of tools to perform adequate quality assurance on this device becomes all the more important for patient safety and treatment effectiveness.

It is also stated in the consensus recommendations of the GEC ESTRO (Groupe Européen de Curiethérapie, European Society for Radiotherapy and Oncology) steering committee, reviewed and approved by the ESTRO ~~ACROP (Advisory Committee for Radiation Oncology Practice), that CXB seems to be an effective method for~~ treating rectal cancer and that it has the potential to preserve the rectum in specific patients. It is considered a safe option with acceptable levels of toxicity, making it particularly beneficial for medically frail or elderly individuals, where choosing an organ-sparing approach with CXB may lead to lower mortality and morbidity compared to surgery. Economic analysis further supports the cost-effectiveness of CXB in potentially operable patients with low rectal cancer [6].

Our study focuses on the comprehensive design and validation of a Monte Carlo (MC) model using the TOPAS Tool for Particle Simulation, tailored to simulate the detailed radiation delivery system of the Papillon+ device with a 25 mm diameter rectal applicator. MC methods, renowned for their accuracy in simulating complex radiation interactions, provide an invaluable tool for understanding and refining the dosimetric characteristics of

these devices. The aim is to enhance the understanding of the dose distribution patterns and to enable reporting or reconstructing of the dose delivered to the target volume and organs at risk. This dose reporting to the target and organs at risk (OAR) is essential for the development of tumour control probability (TCP) and normal tissue complication probability (NTCP) models, which are currently not available. This would further enable clinicians and medical physicists to tailor treatments with heightened accuracy and efficacy in contact x-ray therapy for rectal tumours.

In the subsequent sections, we describe the modelling process and the validations performed. Concerning the validation of the model, simulation results were compared to measurements, including the depth dose on the central axis, the transverse dose profiles and the half-value layer (HVL). After the validation, the x-ray spectrum at different distances from the applicator and a full dose distribution in water were calculated.

Materials and methods

1. Papillon+ device

The Papillon+™ is an eBT device manufactured by Ariane™ Medical Systems (Alfreton, United Kingdom). It contains an x-ray tube with a transmission target made of beryllium coated with tungsten. The tube is cooled with medical-grade white oil. With a tube voltage of 50 kV and a tube current of 2.1 mA, the device delivers low-energy x-rays at a high dose rate of more than 12 Gy per minute at the surface of a water phantom in the case of rectal applications. Specifically for rectal brachytherapy applications, the x-ray source is covered with a nylon flattening filter to filter the exit photon fluence. Three rectal applicators exist with diameters of 20 mm, 25 mm, and 30 mm to further shape the photon fluence. The applicator tubes are open on the end that is placed in contact with the patient. The focus-to-surface distance (FSD) equals 35 mm [7], [8], [9].

Papillon+ data from this study will be compared to an earlier device from the same manufacturer, the Papillon 50™. The device, the dosimetric properties, and its applications were described by Gérard et al. in 2011 [10], Croce et al. in 2012 [11] and Carver et al. in 2013 [12]. A 3D dose distribution, both measured and simulated, was provided by Georgi et al. in 2022 [13].

2. Measurements

a. Depth-dose and transverse dose profile measurements

The depth dose and transverse dose profiles were measured in a solid water phantom of Plastic Water® Low Energy Range (LR) slabs (CIRS, Norfolk, USA) [14]. This material was selected for its excellent water equivalence for low-energy sources in HDR and LDR brachytherapy [15]. Multiple slabs of 15 x 15 cm^2 with different thicknesses (1 mm, 2 mm and 10 mm) were combined to obtain an 8 cm thick phantom. The four lower slabs in the phantom have a thickness of 10 mm and contain a hole in the centre. This allows the insertion of an Exradin A20 (Standard Imaging, Middleton, WI, USA) end-window parallel plate ionisation chamber described by Fulkerson et al. in 2014 [16] connected to a Standard Imaging Max 4000 electrometer. This ionisation chamber was applied to monitor the device's output during the measurements at a fixed depth of 40 mm in the phantom. The ionisation chamber is thus located deeper in the phantom than where the films are located, in order not to distort the measurement with the films. The measurements with the ionisation chamber were performed to apply a correction factor in case of inconsistency. A correction proved unnecessary afterwards. Then EBT3 Gafchromic™ films (Ashland Inc., Wilmington, Delaware, USA), calibrated on a small animal irradiator (SmART-RAD, Precision X-Ray Irradiation, Madison CT, USA) with a 2 mm aluminium (Al) filtration at 60 kVp, were inserted at depths of 0 mm, 5mm, 10 mm, 20 mm and 30 mm (five films per irradiation). The dimensions of the films ranged from 5x5 cm^2 to 9x9 cm^2 to account for the beam divergence. The space around the films was filled with a template (also made from EBT3 films) to cover the air around the film and help with the positioning alignment with the beam's central axis. Irradiations were performed twice for each applicator. For each irradiation, 2000MU was given, which accounts for 20 Gy at the applicator surface. The Gafchromic films were read with FilmqA pro™ v7 analysis software using 3-channel dosimetry. The green channel was selected over the red or blue channel, as it had the steepest curve, i.e. the most sensitive curve. A circular region of interest (ROI) was drawn that was 50 % in area of the size of the irradiated area on the film. The doses were determined by using the mean dose over this ROI. The Gafchromic films of the two irradiations were analysed separately to verify the experimental setup and to check the reproducibility, i.e. the resulted dose was not averaged over the different irradiations. The uncertainty on the film measurements was determined to be 2 %. The uncertainty was based on the consistency maps in filmQA pro™ following the method described by [17]. Figure 1 depicts the measurement setup.

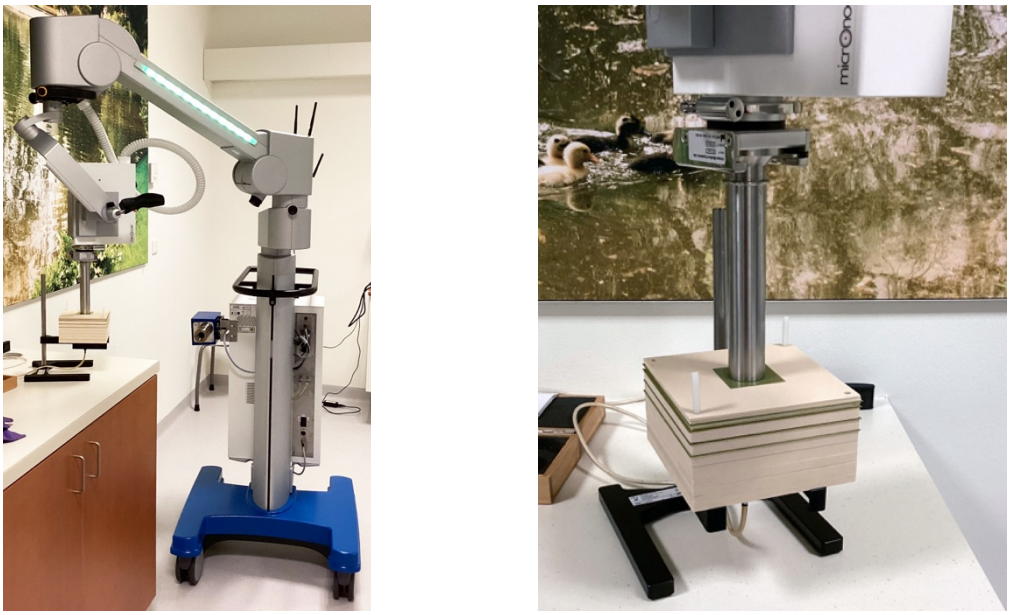

Figure 1: Overview (left) and detailed picture (right) of the depth dose and transverse dose profiles measurement setup. The Papillon+ device with 25 mm diameter rectal applicator in contact with the solid water phantom consisting of Plastic Water LR slabs, loaded with EBT3 films between the slabs and the Exradin A20 ionisation chamber for beam output monitoring at the bottom.

b. Half-value layer measurement

The HVL measurements in this study were performed with a 30 mm diameter rectal applicator in air with a horizontal narrow beam setup, placed in the middle of the treatment room on a carbon tabletop to minimise scatter. A 3 mm thick lead collimator with a 20 mm round aperture is positioned 15 cm from the applicator surface. Calibrated PTW aluminium HVL sheets were placed at another 15 cm from the first collimator together with a second 1 mm thick lead collimator with a 20 mm round aperture. A PTW 23342 (PTW Dosimetry, Freiburg, Germany) parallel plate ionisation chamber with a polyethene build-up cap is positioned 15 cm from the HVL sheets. The distances were selected to optimise the signal-to-noise ratio. The measurement setup is schematically represented in Figure 2. The first HVL was defined as the thickness of aluminium needed to halve the air kerma. If not explicitly specified, the abbreviation HVL in this manuscript refers to the first HVL.

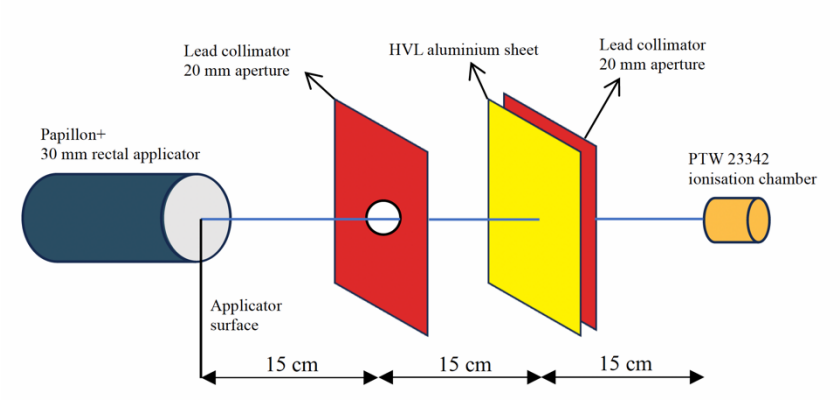

Figure 2: Schematic representation of the HVL measurement setup. Lead collimator (red) at 15 cm from the applicator surface (blue), aluminium HVL sheet (yellow) and second collimator (red) at 15 cm from the first collimator and PTW 23342 ionisation chamber (orange) at 15 cm from the HVL sheet.

The measurement setup of the manufacturer is different. Ariane Medical Systems performs the HVL measurement also with the 30 mm rectal applicator, but in a broad-beam setup (without a collimator). A Radcal® 10X6-6M mammography ionisation chamber [18] was applied, as it provided a good energy response for its intended purpose. An applicator-detector distance of 15 cm was used, with the aluminium HVL sheets placed half-way in a dedicated holder.

3. Monte Carlo simulations

a. Monte Carlo code

The Monte Carlo toolkit TOPAS was used for this research, version 3.9 (release date December 16, 2022), which relies on GEANT4 version 10.7 patch 03 (November 19, 2021) [19], [20]. In GEANT4, the physics configuration is accomplished by the 'Physics Lists'. These lists determine the particles and physics processes included in the simulation and the specific cut-offs and options to be utilised. As this study aims to simulate the production and transport of low-energy x-rays within an energy range up to 50 keV, the TOPAS module name *G4em-penelope* was selected, referring to the physics model with Geant4 Class Name *G4EmPenelopePhysics*. This physics list is based on data from the Penelope MC code [21] (version 2008) and includes electrons, positrons and photons from 250 eV to 1 GeV [22] [23]. This was preferred over the Livermore and the Standard EM Physics model because of its better performance for the bremsstrahlung production [24]. When examining low-energy x-rays, it is important to note that the primary method of energy transmission to secondary electrons is through the photoelectric effect. However, uncertainties regarding photoelectric cross sections below 100 keV can significantly contribute to type B uncertainties [25]. Recently, Valdes-Cortez et al. [26] concluded that in

this low-energy range, type B uncertainties stemming from different cross-section implementations are more dominant than type A uncertainties or other sources of type B uncertainties (like scoring volume averaging or manufacturing tolerances). According to their work, a type B uncertainty (k = 2) ranging from 1.2 to 1.7% was estimated for the absorbed dose below 50 keV.

In the physics settings of TOPAS, the parameters Auger electron production, Auger cascade and fluorescence were enabled. The default transport cut-off was reduced to 1 μm for all particles. Variance reduction techniques were applied. This includes the split of secondary photons created in the target component by a bremsstrahlung process. The bremsstrahlung split factor was set to 100. A directional filter was further applied to ensure that this variance reduction technique only affects particles travelling in the direction of the applicator surface.

The simulations were performed on the Tier 2 cluster of the Flemish Supercomputer Center, more specifically on the Skylake nodes running 2 Xeon Gold 6140 CPUs, operating at 2.3 GHz each [27].

c. Model design

The MC model was developed based on the blueprints and CAD models of the device obtained by private communication with Ariane Medical Systems. However, the exact geometry and material compositions of the x-ray source and applicators are proprietary. The MC model includes the bare x-ray device in combination with the 25 mm diameter rectal applicator. Phase space files were created at the level of the applicator surface to be used in subsequent simulations. A representation of the MC model with a rectal applicator (yellow) and nylon flattening filter (red) can be seen in Figure 3. The FSD equals 35 mm.

The world surrounding the source model consists of air. For this, the standard material composition, density and mean excitation energy defined in TOPAS and GEANT4 was used, which corresponds to the definition by the National Institute of Standards and Technology (NIST) [28] [29].

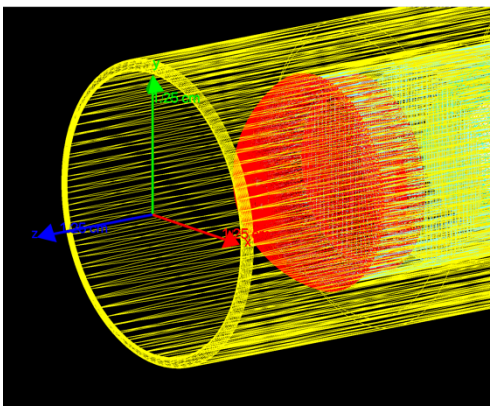

Figure 3: MC model of the Papillon+ device with 25 mm diameter rectal applicator. The rectal applicator

(yellow) and nylon flattening filter (red) can be recognised. The arrows are indicating 12.5 mm

d. Depth-dose and transverse dose profile simulations

For the depth dose and transverse dose profile simulations, Plastic Water LR was simulated by creating a custom material with a density of 1.029 g/cm^3 and elemental compositions and corresponding mass fractions, as shown in Table 1 [15]. The absorbed dose-to-water was scored in 1 mm^3 voxels. The number of histories in each simulation was adapted to obtain an uncertainty of lower than 1 % in the voxels of interest.

Table 1: Elemental composition and corresponding mass fraction for Plastic Water LR used in the MC simulations.

Element	Mass fraction
Hydrogen	0.0791
Carbon	0.5362
Nitrogen	0.0174
Oxygen	0.2721
Magnesium	0.0929
Chlorine	0.0023

e. X-ray spectrum simulations and HVL determination

The x-ray fluence was scored in 0.1 keV energy bins in a cylindrical scoring volume with a radius of 15 mm and thickness of 1 mm, positioned in contact with and at distances in air of 5, 15, 30, 45 and 50 cm from the applicator surface of the rectal applicator. The number of histories in the simulation was adapted to obtain an uncertainty of lower than 1% in the energy bins. The first and second HVL values are derived from the x-ray spectra using the equation proposed by Verhaegen et al. (1999) [30], based on the mass attenuation coefficient for aluminium and mass energy-absorption coefficients for air [31]. The second HVL refers to the additional thickness of the absorber that must be added on top of the first HVL to reduce the initial air kerma to 25 %.

f. Simulated 2D dose distribution

A complete dose distribution was also simulated of the Papillon+ with 25 mm diameter rectal applicator in water. For this, the absorbed dose-to-water was scored in (liquid) water in 1 mm^3 voxels. For the medium, the standard definition of water as defined in TOPAS and GEANT4 was used, which corresponds to the definition of NIST [28] [29]. The dose was normalised to the dose at the surface. A plane through the central axis was extracted from the 3D dose distribution and isodose lines were added for the visualisation.

Results

1. Depth-dose profile

The depth dose profiles, normalised to the surface dose, are represented in Figure 4. The depth dose curves for the MC model with the 25 mm diameter rectal applicator, simulated in both Plastic Water LR (dark blue solid curve) and regular water (clear blue dashed curve), overlap within the uncertainty of the simulations. Film measurements performed with the 20 mm, 25 mm and 30 mm diameter rectal applicator are visualised with orange, yellow and purple circular markers, respectively. Error bars were added to the measurements with the 25 mm applicator (omitted for the other measurements to improve visibility). For the three different rectal applicators, the measured depth dose profiles show no significant differences. An excellent agreement within ± 2 % was achieved between the MC simulations and the measurements. This is within the combined measurement and simulation uncertainty.

When the measured and simulated depth dose curve of the Papillon+ are now compared to the measured depth dose curve of the Papillon 50 [13], both in liquid water, it can be noted that the depth dose curve for the Papillon+ is significantly steeper than the depth dose curve of the Papillon 50.

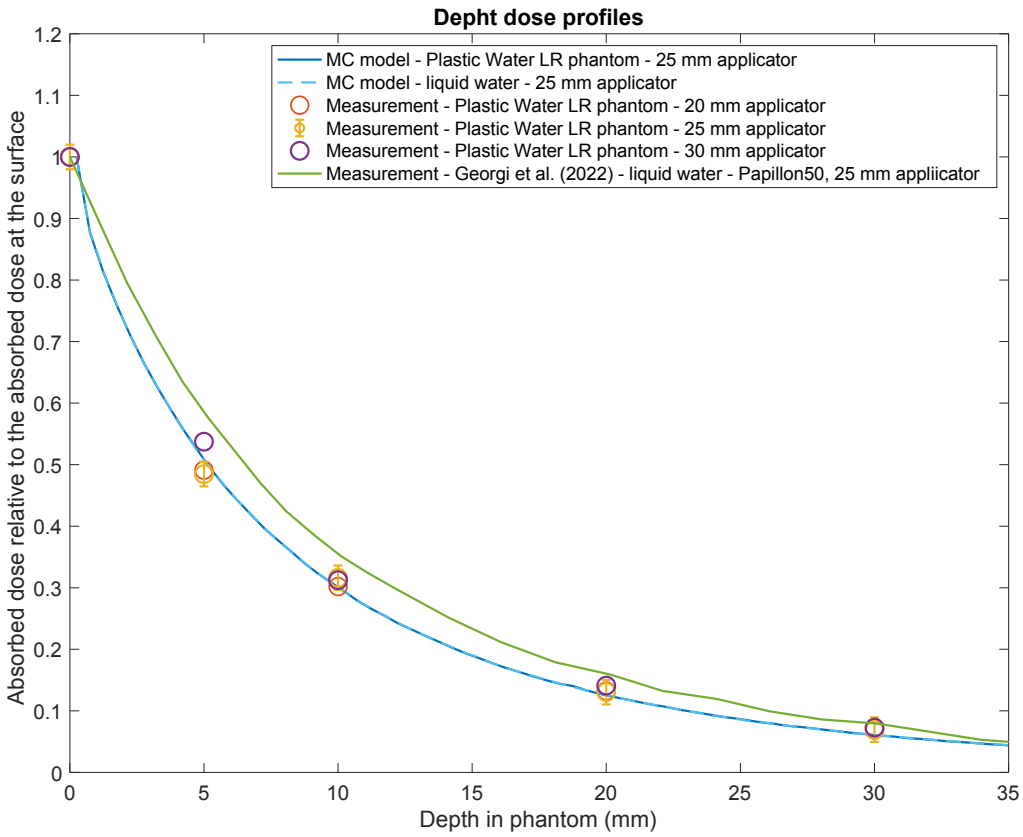

Figure 4: Measured and MC simulated depth dose curves of the Papillon+ device.

4. Transverse dose profiles

Figure 5 represents, for each case, two transverse dose profiles perpendicular to each other, referred to as x and y, in contact with the rectal applicator and at a depth of 10 mm in a Plastic Water LR phantom. The displayed data are for the rectal applicator with a diameter of 25 mm. This figure compares film measurements (indicated with dashed lines) to the simulated data (shown with solid lines). The transverse dose profiles were normalised to the average dose of the central 20 mm at the surface.

For both the profiles in contact with the applicator and at 10 mm depth in the phantom, a close agreement can be observed between the simulations and the measurements for each direction. The difference between the measurements and simulations averages 3.1 % for the transverse dose profiles in contact with the applicator and 1.7 % for the transverse dose profiles at 10 mm depth. The profiles in contact have a width (defined as the full width at half maximum, FWHM) of 25.2 mm for the measurements and 25.4 mm for the simulations, averaged for the x and y directions. This corresponds closely (< 1.6 %) to the actual diameter of the applicator. A homogeneous dose distribution for the profiles in contact with the applicator can be noticed. Only the measured dose profile in contact and in the x-direction (Figure 5 (left), blue dashed line) looks slightly different. Even considering the measurement noise, this profile appears slightly skewed This is most probably due to an inaccuracy in the positioning of the film with respect to the applicator.

For the transverse profiles at 10 mm depth, a FWHM of 32.8 mm and 32.4 mm, averaged for the x and y directions, are calculated for the measurements and simulations, respectively. This means the beam profile at 10 mm depth is wider than at contact. This corresponds to a diverging beam. It can also be noted that the profile becomes less flat compared to the situation in contact. When the transverse dose profiles at 10 mm depth are compared with those in contact with the applicator, a three times lower dose is obtained at 10 mm depth. This is compatible with the dept dose curve as discussed earlier.

Table 2 summarises the width of the measured and simulated transverse dose profiles at different depths in the plastic water LR phantom. The difference in the FWHM between the measurements and simulations is less than 1 %.

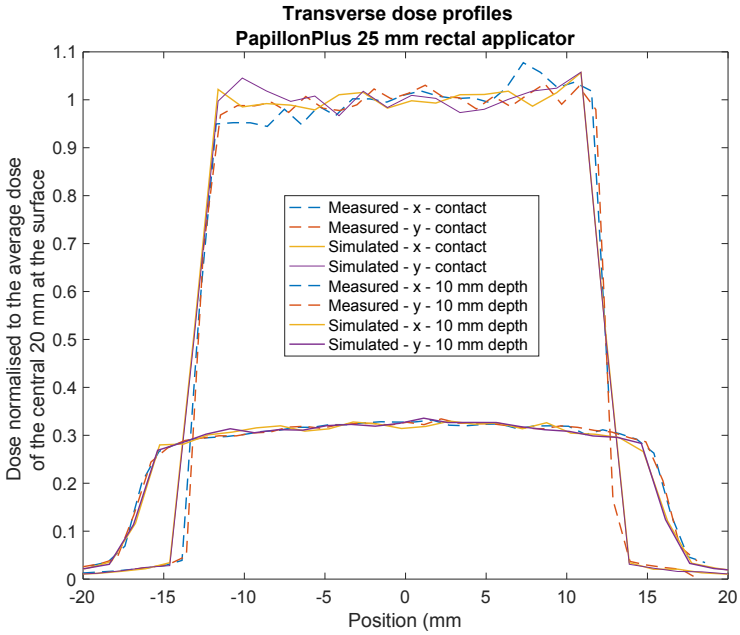

Figure 5: Transverse dose profiles of Papillon+ with 25 mm diameter rectal applicator in x and y direction, in contact with the applicator and at 10 mm depth in Plastic Water LR phantom, measured (dashed line) and simulated (solid line).

Table 2: Width of the measured and simulated transverse profiles, defined as FWHM (full width at half maximum) at different depths in plastic water LR

Depth in the phantom (mm)	**Measurement FWHM (mm)**	**Simulation FWHM (mm)**	**Relative difference of the measurement compared to the simulation (%)**
0	25.2	25.4	-0.69
5	28.8	28.8	0.26
10	32.5	32.4	0.12
20	39.7	39.5	0.40
30	46.6	46.4	0.44

5. X-ray spectrum

The simulated x-ray spectra of the Papillon+ with a 25 mm diameter rectal applicator at different distances in air from the applicator surface are represented in Figure 6. The simulated spectrum comprises a continuous bremsstrahlung spectrum up to 50 keV and characteristic x-ray peaks. Based on the characteristic x-ray peaks,

the following elements were identified: tungsten, originating from the x-ray target and chromium, iron, nickel, and molybdenum originating from the stainless-steel body of the collimator [32]. The different characteristic x-ray peaks with corresponding elements and transitions are summarised in Table 3. In Figure 6, the intensity of the characteristic x-ray peaks decreases, and the Bremsstrahlung spectrum slightly shifts towards the higher energies with increasing distance from the applicator.

The mean x-ray energy calculated from the simulated x-ray spectra at different distances in air is represented in Figure 7. It can be observed that the mean x-ray energy increases slightly with increasing distances from the applicator surface. The increase is most noticeable close to the applicator and diminishes with increasing distance.

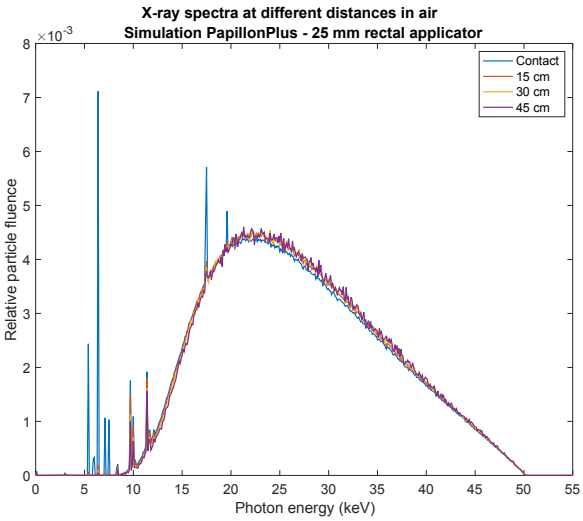

Figure 6: Simulated x-ray spectrum of Papillon+ with 25 mm diameter rectal applicator at different distances in air from the applicator surface.

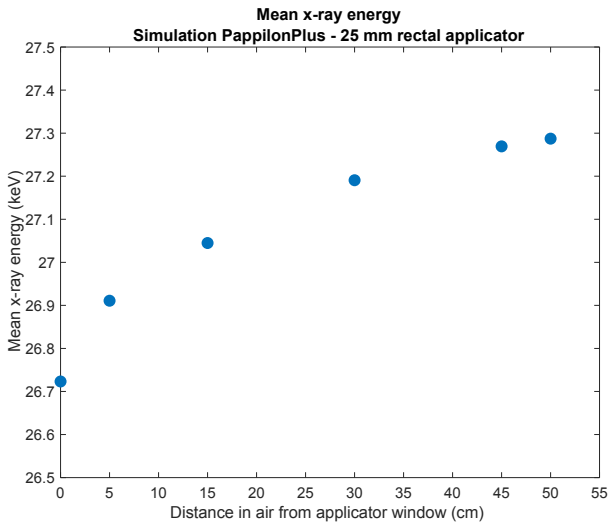

Figure 7: Mean x-ray energy of the Papillon+ with 25 mm diameter rectal applicator derived from simulated x-ray spectra in function of the distance in air from the applicator surface.

Table 3: Characteristic x-ray peaks, extracted from simulated x-ray spectrum of Papillon+ with 25 mm diameter rectal applicator, with corresponding elements and transitions [32].

X-ray energy (keV)	Element	Transition
5.4	Cr	*Kα1*
6.4	Fe	*Kα1*
7.1	Fe	*Kβ1*
7.5	Ni	*Kα1*
8.4	W	*Lα1*
9.7	W	*Lβ1*
10	W	*Lβ2*
11.3	W	*Lγ1*
17.5	Mo	*Kα1*
19.6	Mo	*Kβ1*

with K or L, the destination atomic level of the electron

with α, β or γ, the origin of the electron, respectively one, two or three atomic levels higher

with 1 or 2, the difference in the original electronic orbitals' energy level.

6. Half-value layer

Table 4 compares the measured and simulated HVLs. For the 30 mm diameter rectal applicator, an HVL of 0.765 mm Al was measured. This is slightly larger than the value measured by Ariane Medical Systems (private communication) but note the considerable uncertainty on the reported value. An MC model only exists for the 25 mm applicator. Simulation results with an applicator diameter of 25 mm were compared with measurement results with an applicator diameter of 30 mm. From the simulated x-ray spectrum, an HVL of 0.614 mm Al and 0.653 mm Al were obtained at 15 cm and 45 cm in air, the same applicator-detector distances as the measurements performed by the manufacturer and this study, respectively. When both simulation results are compared to the measured results at the corresponding distances, it can be observed that the MC model agrees within 5.5% with the measurement data from the manufacturer, where the simulated HVL value is approximately 15 % smaller than our own measured value.

Hereafter, the results of the MC simulations are considered in more detail. Figure 8 represents the first and second HVL derived from the simulated x-ray spectra at different distances in air from the applicator surface. It can be observed that the simulated HVL values (both first and second) increase with increasing distances from the applicator surface. The increase is most noticeable close to the applicator and diminishes with increasing distance. The second HVL is approximately double of the first HVL close to the applicator. As the distance increases, the thickness of the second HVL reduces to about 2/3rd of the first HVL.

Table 4: HVL (mm Al) of the Papillon+.

Diameter of rectal applicator:	**25 mm**	**30 mm**
Measurement		0.765 ± 0.005
Measurement data Ariane		0.65 ± 0.5
Simulation	0.614 (at 15 cm in air from applicator window) 0.653 (at 45 cm in air from applicator window)	

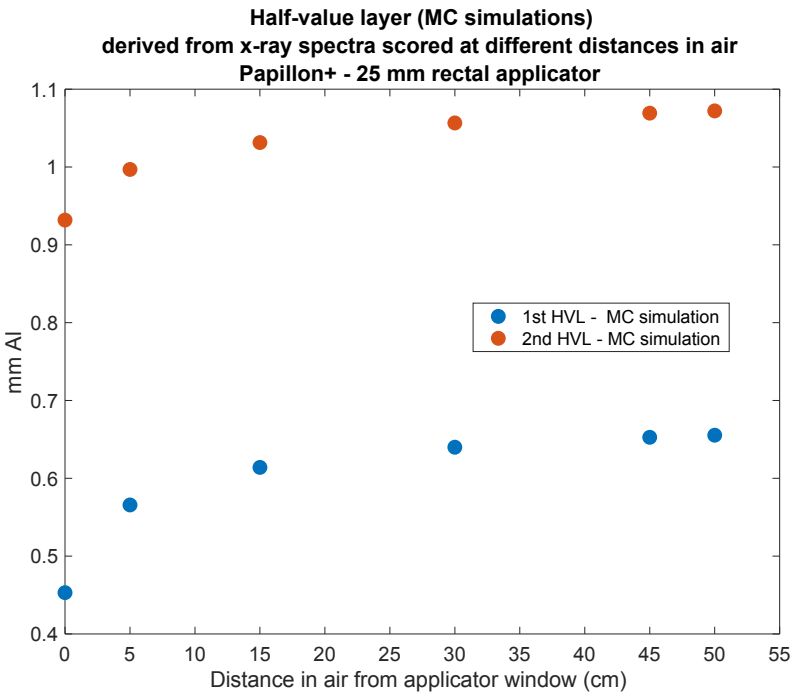

Figure 8: First (blue markers) and second (orange markers) HVL values in mm Al derived from the simulated x-ray spectra of the Papillon+ with 25 mm diameter rectal applicator at different distances in air from the applicator surface.

7. Summary measurements and comparison with Papillon 50 device

Table 5 provides an overview of the measured dosimetric properties of the Papillon+ device for the three different sizes of rectal applicators, where available. This summary includes the focus to surface distance, the tube current and voltage, the mean photon energy, the HVL, the depth of 50% dose and the ratios of the dose at 5mm and 10 mm depth, respectively to the surface dose. These values are compared to the dosimetric characteristics of the Papillon 50 device, as published by Gérard et al. in 2011 [10], Croce et al. in 2012 [11] and Georgi et al. in 2022 [13].

As summarised in Table 4, both devices deliver a 50 kVp photon spectrum but different dosimetric properties can be expected due to their difference in source design, applicator geometry and corresponding filtration. A significant difference between the two devices is the focus surface distance, which is 39 mm for the Papillon+, compared to 29 mm for the Papillon 50. The latter is expected to be a dominating effect. The mean photon energy of the Papillon+ appears to be slightly higher than that of the Papillon 50. Also, the HVL is larger for the Papillon+ compared to the Papillon 50.

It is challenging to compare the measured depth doses of the Papillon 50 and the Papillon+, as they were measured in different materials, i.e. PMMA for [11] or liquid water for [13] for the Papillon 50 and Plastic Water LR for the Papillon+. As can be seen in Table 5, the depth of the 50 % dose is less deep for the Papillon+ than for the Papillon 50. Also, the ratios of the dose at 5 and 10 mm to the surface dose, respectively, are smaller for the Papillon+ than for the Papillon 50. This is compatible with the previous findings on the depth dose profiles. This is, however, inconsistent when the HVL and mean photon energy are studied. The HVL and the mean photon energy of the Papillon+ are larger than of the Papillon 50.

Table 5: (Measured) dosimetric properties of the Papillon+ compared to Papillon 50. All data reported for the Papillon 50 device are from the three mentioned papers.

	Papillon 50						**Papillon+**		
Device:	Gérard et al., 2011 [10]		Croce et al., 2012 [11]			Georgi et al., 2022 [13]	measurements in this study		
Diameter of rectal applicator (mm)	22	30	22	25	30	25	20	25	30
Focus-to-surface distance (mm)	29						35		
Tube current (mA)	2.7						2.1		
Tube voltage (kV)	50						50		
Mean photon energy (keV)	26.5		-			-	27.2 (5 cm in air) – 27.5 (50 cm in		
HVL (mm Al)	0.55	0.57	-	-	-	-	-	-	0.76
Depth of 50 % dose (mm)	6.5	7	6.0	6.6	7.1	6.6	4.9	4.7	5.6
Ratio dose at 5 mm depth to surface dose	0.55	0.6	-	-	-	-	0.49	0.48	0.54
Ratio dose at 10 mm depth to surface dose	0.34	0.38	-	-	-	-	0.30	0.32	0.31

8. Simulated 2D dose distribution

Figure 9 illustrates the simulated dose distribution in water in two dimensions across a plane on the beam's central axis. The absorbed dose is normalised to the dose at the surface. Isodose lines were added every 10%.

It can be noted that the dose at a lateral distance equal to 0 mm as a function of depth is consistent with the simulated depth dose profiles shown in Figure 4, as expected. As with the transverse dose profiles, it can also be seen that the transverse dose profiles are flatter the closer to the applicator surface and that the transverse dose profiles become more convex as the depth increases. It is also observed that the radius increases with depth, which is compatible with a diverging beam.

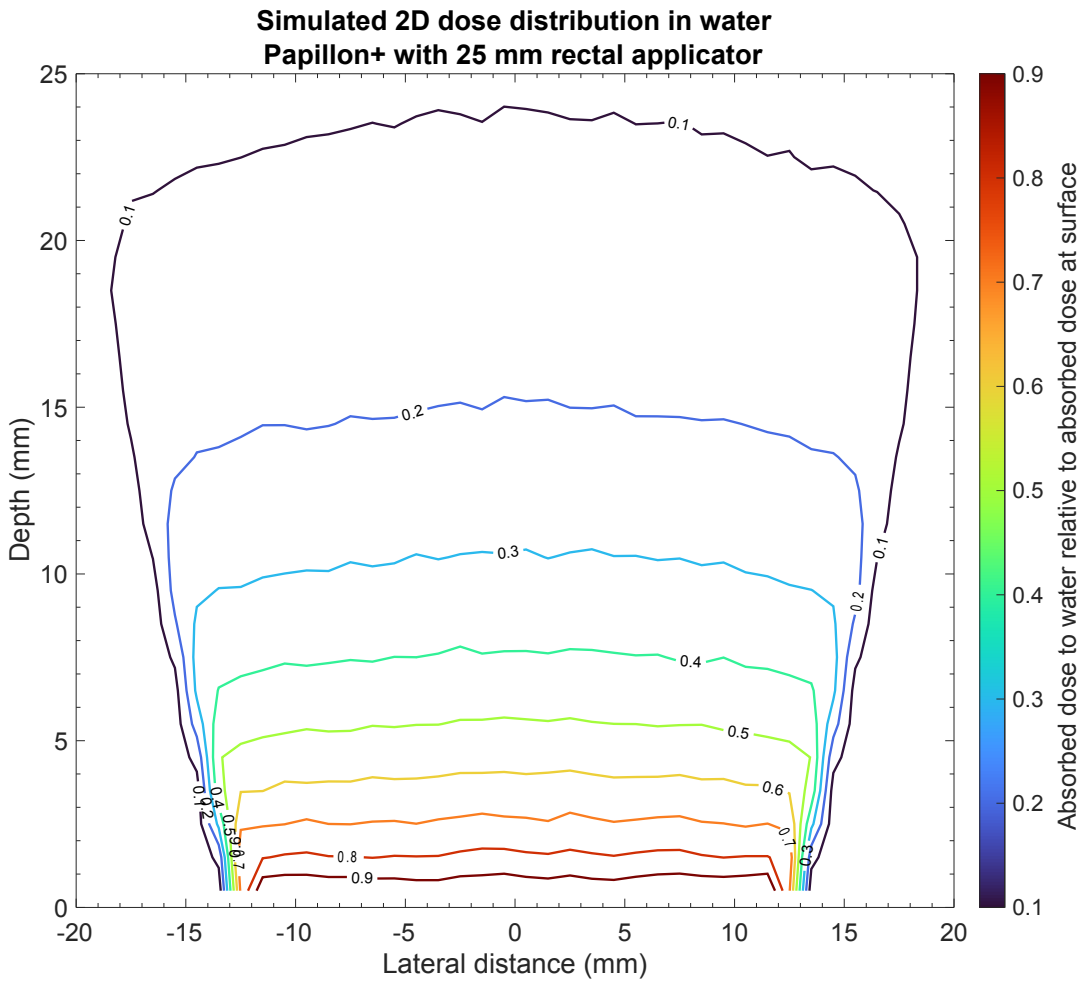

Figure 9: Two-dimensional dose distribution simulated in liquid water of the Papillon+ with 25 mm diameter rectal applicator including isodose lines, representing the absorbed dose relative to the absorbed dose at the surface.

Discussion

This study aimed to produce an MC model of Ariane Medical Systems' Papillon+ CXB device with a 25mm diameter rectal applicator. The MC model was validated with depth dose and transverse dose profile measurements using EBT3 Gafchromic films positioned in a Plastic Water LR phantom. There is an excellent agreement within ± 2 % noted for the measured and simulated depth dose curves on the central axis for the 25 mm diameter rectal applicator. The depth dose curve was simulated in both Plastic Water LR (to compare to measurements) and in liquid water. Here, the curves in both materials match within the uncertainty of the simulation, which indicates the perfect water equivalence of the Plastic Water LR material for this photon energy range, as was expected based on the results of Schoenfeld in 2017 [15]. Considering the measured depth dose curves, no considerable difference can be noted on the central axis between the three applicators with diameters

20 mm, 25 mm and 30 mm. Likewise, the simulated and measured transverse dose profiles agree to a high extent, both in contact with the applicator (on average 3.1 %) and at 10 mm depth (on average 1.7 %). A uniform dose distribution at the surface of the applicator can be noted for the Papillon+ with a 25 mm diameter rectal applicator.

The model was further validated by comparing the HVLs. It should be noted here, however, that the measurement was performed with the 30 mm applicator, whereas for the simulation, only a model is available for the 25 mm diameter rectal applicator. This can be explained as follows. The HVL measurements are part of the initial calibration chain in accordance with Report 10 of the Netherlands Commission on Radiation Dosimetry (NCS10) [33]. Following this procedure, a free-in-air measurement must be performed in the Papillon+ beam to compare to the free-in-air measurement in the primary standards lab where the ionisation chamber was calibrated. The rectal applicators produce field diameters that are much smaller than those used in the calibration at the standards lab. To minimise the effects from the field size and to approach as much as possible the same detector scatter in the Papillon+ beam, the rectal applicator with the largest diameter, 30 mm diameter, was selected to translate the free-in-air calibration to the full-scatter dose at the end of an applicator. The other applicator diameters are compared to the 30 mm diameter applicator in full-scatter conditions. Based on the agreement between the depth dose profile measurements on the central axis of the different applicators, it is decided that the difference in applicator diameter for the measurement and simulations could only have a minimal impact on the HVL results obtained.

A fair agreement within 15 % between our own measurement and the simulation can be observed, with 0.765 mm Al and 0.653 mm Al, respectively. It should be noted, however, that the device's flattening filter was modified during a technical service intervention, so it may be slightly different from the description provided in the blueprint, used for the MC modelling. This may explain a difference in the simulated and measured HVL. A close agreement withing 5.5 % between the measurement of the manufacturer and the simulation can be noted, with 0.65 mm Al and 0.614 mm Al, respectively. A comparison of our own measured HVL value and the HVL value provided by Ariane Medical Systems is difficult to perform, due to the large measurement uncertainty reported by the manufacturer, the different applicator surface to detector distances, the fact that they use a broad-beam (without collimators), while in our study a narrow beam geometry was applied, following NCS10 [33] and the unknown influence of the technical intervention to the flattening filter, as mentioned earlier.

The simulated HVL was derived from the x-ray spectrum scored at the exact distances between the source and ionisation chamber as used in the HVL measurement, which were 15 cm and 45 cm. As noted earlier, there is a

notable beam hardening in air due to the soft x-ray energy spectrum and characteristic photons absorbed in air. This is why, in Figure 8, which represents the HVL based on the simulated x-ray spectrum at different distances in air from the applicator surface, the HVL first sharply increases before gradually reaching a plateau as the distance in air increases. It illustrates the extreme sensitivity of the measurement setup.

The MC model shows a rather soft x-ray spectrum. The simulated spectrum comprises a continuous bremsstrahlung spectrum up to 50 keV and characteristic x-ray peaks originating from the x-ray target (W) and the stainless-steel body of the applicator (Cr, Fe, Ni and Mo). The mean photon energy equals 26.7 keV at the level of the applicator surface. In Figure 7, representing the mean photon energy as a function of the distance in air from the applicator, a prominent beam hardening in air can be noticed. The mean photon energy increases to approximately 27.3 keV at 50 cm from the applicator. This beam hardening can also be observed in Figure 6, representing the x-ray spectra at different distances in air from the applicator. Here, the Bremsstrahlung spectrum slightly shifts towards the higher energies as the distance increases. In the same figure, the intensity of the characteristic x-ray peaks substantially decreases as the distance in air increases. This is because characteristic x-rays are emitted isotropically (and thus follow the inverse square law), while bremsstrahlung is emitted mainly forward in the case of a transmission target. Some of the characteristic x-ray peaks come from the applicator and are thus generated closer to the scoring volume, compared to bremsstrahlung photons from the target. Also because of this, these characteristic x-ray photons behave more isotropically.

The soft x-ray spectrum is also apparent in the depth dose measurements. For example, for the 25 mm applicator, the depth of the 50% dose is equal to 4.7 mm, and the ratio of the dose at 10 mm depth to the surface dose is equal to 0.32. Also, the simulations of the HVL illustrate the soft x-ray spectrum, i.e. the second HVL is approximately equal to double the first HVL. Based on the measured and simulated depth dose curves, it can be concluded that the Papillon+ delivers a softer x-ray spectrum compared to the Papillon 50 [10], [11]. This, however, does not correspond when the HVL measurements of the Papillon+ from our study are considered. The HVL obtained by Gérard et al. for the Papillon 50 system (0.57 mm Al for the 30 mm applicator) [10] is lower than the measured (0.76 mm Al for the 30 mm applicator) and simulated HVL (0.65 mm Al for the 25 mm applicator) for the Papillon+ obtained as part of our study, which would indicate that the Papillon+ has a harder spectrum compared to the Papillon 50. This contradicts the earlier conclusions. Since [10] does not provide any details on the method and experimental setup used to determine the HVL and given that the major beam hardening in air considerably influences the measurement, as discussed earlier, this is not considered further. There is also no further comparison made between the simulated x-ray spectrum of the Papillon+ (Figure 6) and

the measured x-ray spectra of the Papillon 50 published by [10] and [11], because, on the one hand, these spectra seem to be not corrected for detector response as absorption edges of cadmium and telluride of the detector are noticeable in the spectrum and, on the other hand, detailed information on the detector used was not available to include in our simulation. We do not have a detector with a corresponding correction curve for detector response available to perform spectral measurements.

The MC model is developed based on the blueprints and CAD models obtained from the device manufacturer. We started with the modelling of the device with the 25 mm diameter rectal applicator and performed thorough comparisons. Due to the MC model's modular design, the other applicators' CAD models can easily be added to this MC model. A corresponding depth dose profile is expected on the central axis for the simulations of the 20 mm and 30 mm diameter applicators, as the measurements observe a close agreement between the depth profiles for the three applicators. The transverse dose distribution will change if the diameter of the applicator changes.

In this study, depth dose, transverse dose and HVL measurements were performed to validate the MC model. It is important to carefully check all these parameters when commissioning any new device, as there may be minor differences between the devices.

The developed MC model allows for the simulation of the absorbed dose on a high spatial resolution in three dimensions. For example, Figure 9 illustrates the 2D dose distribution in water in depth of a plane on the beam's central axis. It should be noted that this dose distribution is simulated in (homogeneous) water. Heterogeneities were not considered. In the case of rectal cancer, it should be investigated whether a rectal tumour, as well as the different layers of the rectum wall (mucosa, submucosa, muscularis and adventitia), can be adequately approximated by water. However, the MC model allows further detailing of the simulation and associated dose distribution by adjusting and matching the size and composition of the different structures and tissues. This is one of the major advantages of the MC model. A follow-up study will further explore the dose reporting to the target and the OAR to gain insight into the delivered dose, local control and toxicity in clinical cases. A more advanced dose calculation can ensure the improvement of the radiotherapy treatment.

Conclusion

This study successfully developed and validated an MC model for Ariane Medical Systems' 50 kV Papillon+ eBT device with a 25 mm diameter applicator. This device is used for the contact treatment of rectal tumours. The validation process involved measurements of depth and transverse dose profile using EBT3 gafchromic films in a Plastic Water LR phantom. The results demonstrated excellent agreement within ± 2 % between the

measured and simulated depth dose curves for the 25 mm rectal applicator. Transverse dose profile measurements exhibited a high level of agreement between the simulation and measurements, on average 3.1 % and 1.7 % in contact with the applicator and at 10 mm depth, respectively. The model's validation extended to the HVL, showing a close agreement of 5.5 % between the measurement and simulation.

The MC model has a flexible and modular structure, allowing various applications, including quality assurance, treatment optimisation and dose reconstruction. The MC model characterised the device's x-ray spectrum, highlighting a soft energy spectrum with a notable beam hardening in air with characteristic photon peaks readily absorbed in air but may play a role in the dose in the tissue in direct contact with the applicator. The simulated 2D-dose distribution additionally demonstrated a homogeneous dose distribution at the surface of the applicator. Future work will explore the impact of these findings on clinical cases, ensuring CXB applications continue to improve.

Acknowledgements

We gratefully acknowledge the financial support provided by the Special Research Fund (Bijzonder Onderzoeksfonds, BOF). This research was made possible through the grant BOF19DOC28 awarded to Dries Colson.

We further thank Ariane Medical Systems for providing the data and discussion that made it possible to create the MC model.

We also thank prof. Jean-Pierre Gérard for discussion.

The PRISM-eBT project with project number 18NRM02 has received funding from the EMPIR programme co-financed by the Participating States and from the European Union’s Horizon 2020 research and innovation programme.

The computational resources and services used in this work were provided by the VSC (Flemish Supercomputer Center), funded by the Research Foundation - Flanders (FWO) and the Flemish Government.

Conflicts of interest

The authors declare that they have no known competing financial interests or personal relationships that could have appeared to influence the work reported in this paper.

References

[1] C. C. Park, A. Bevan, M. B. Podgorsak, J. Pouliot and S. S. Yom, “Emerging Technology Committee Report on Electronic Brachytherapy,” Electronic Brachytherapy Working Group Evaluation Subcommittee of ASTRO"s Emerging Technology Committee, s.l., 2008.

[2] D. Eaton, “Electronic brachytherapy - current status and future directions,” *British Journal of Radiology,* vol. 88, no. 1049, p. 20150002, 2015.

[3] P. Ramachandran, “New era of electronic brachytherapy,” *World Journal of Radiology,* vol. 9, no. 4, pp. 148-154, 2017.

[4] D. Hitova-Topkarova, V. Payakova, D. Kostova-Lefterova, M. Ivanova, M. Vasileva-Slaveva and A. Yordanov, “Electronic brachytherapy for gynecological cancers — a systematic review,” *Reports of Practical Oncology and Radiotherapy,* vol. 28, no. 1, pp. 79-87, 2023.

[5] J.-P. Gerard, N. Barbet, R. Schiappa, N. Magné, I. Martel, L. Mineur, M. Deberne, T. Zilli, A. Dhadda and A. Myint, “Neoadjuvant chemoradiotherapy with radiation dose escalation with contact x-ray brachytherapy boost or external beam radiotherapy boost for organ preservation in early cT2–cT3 rectal adenocarcinoma (OPERA): a phase 3, randomised controlled trial,” *The Lancet - Gastroenterology & Hepatology,* vol. 8, no. 4, pp. 356-367, 2023.

[6] A. J. Stewart, E. J. Van Limbergen, J.-P. Gerard, A. L. Appelt, F. Verhaegen, M. Berbee, T. Vuong, C. Brooker, T. Rockall and A. Sun Myint, “GEC ESTRO ACROP consensus recommendations for contact brachytherapy for rectal cancer,” *Clinical and Translational Radiation Oncology,* vol. 33, pp. 15-22, 2022.

[7] Ariane Medical Systems, “PapillonPlus X-ray Brachyterhapy Systems,” Ariane Medical Systems, 2019. [Online]. Available: https://www.arianemedicalsystems.com. [Accessed 1 June 2023].

[8] Ariane Medical Systems, “Improving X-Ray brachytherapy treatment using the Papillon+™,” News-Medical, 23 March 2023. [Online]. Available: https://www.news-medical.net/whitepaper/20220215/Using-the-Papillon2be284a2-to-Improve-X-ray-Brachytherapy-Treatment.aspx. [Accessed 1 June 2023].

[9] A. Sun Myint, A. Stewart, J. Mills, R. Stripadam, K. Whitmarsh, R. Roy, A. Franklin and A. Dhadda, “Treatment: the role of contact X-ray brachytherapy (Papillon) in the management of early rectal cancer,” *Colorectal Disease,* vol. Suppl 1, pp. 45-52, 2019.

[10] J.-P. Gérard, A. S. Myint, O. Croce, J. Lindegaard, A. Jensen, R. Myerson, J.-M. Hannoun-Lévi and S. Marcie, “Renaissance of contact x-ray therapy for treating rectal cancer,” *Expert Rev.Med. Devices,* vol. 8, no. 4, pp. 483-492, 2011.

[11] O. Croce, S. Hachem, E. Franchisseur, S. Marcié, J.-P. Gérard and J.-M. Bordy, “Contact radiotherapy using a 50 kV X-ray system: Evaluation of relative dose distribution with the Monte Carlo code PENELOPE and comparison with measurements,” *Radiation Physics and Chemistry,* vol. 81, pp. 609-617, 2012.

[12] A. Carver, A. Gately, R. Clements and A. Nahum, “Monte Carlo dosimetry for the Papillon P50 contact radiotherapy and IORT device,” *Radiotherapy and Oncology,* vol. 109, pp. 367-369, 2013.

[13] P. Georgi, G. Kertzscher, L. Nyvang, J. Šolc, T. Schneider, K. Tanderup and J. G. Johansen, “Toward a 3D dose verification of an electronic brachytherapy source with a plastic scintillation detector,” *Medical Physics,* vol. 49, pp. 3432-3443, 2022.

[14] Computerized Imaging Reference Systems, Inc., “Plastic Water(R) LR Low Energy Range,” 2010. [Online]. Available: https://www.cirsinc.com/wp-content/uploads/2020/12/PWLR-UG-062119.pdf.

[Accessed 25 May 2023].

[15] A. A. Schoenfeld, M. Thieben, D. Harder, B. Poppe and N. Chofor, "Evaluation of water-mimicking solid phantom materials for use in HDR and LDR brachytherapy dosimetry," *Physics in Medicine and Biology,* vol. 62, pp. N561-N572, 2017.

[16] R. K. Fulkerson, J. A. Micka and L. A. DeWerd, "Dosimetric characterization and output verification for conical brachytherapy surface applicators. Part I. Electronic brachytherapy source," *Medical Physics,* vol. 41, no. 2, pp. 022103-1-21, 2014.

[17] A. Micke, D. F. Lewis and X. Yu, "Multichannel film dosimetry with nonuniformity correction," *Medical Physics,* vol. 38, no. 5, pp. 2523-2534, 2011.

[18] Radcal Corporation, "10X6-6M - The Dedicated Mammography Chamber," 12 7 2011. [Online]. Available: https://radcal.com/wp-content/uploads/2016/10/radcal-10X6-6M-chamber-spec-sheet.pdf. [Accessed 1 December 2023].

[19] J. Perl, J. Shin, J. Schumann, B. Faddegon and H. Paganetti, "TOPAS: an innovative proton Monte Carlo platform for research and clinical applications," *Medical Physics,* vol. 39, no. 11, pp. 6818-6837, 2012.

[20] B. Faddegon, J. Ramos-Méndez, J. Schümann, A. McNamara, J. Shin, J. Perl and H. Paganetti, "The TOPAS Tool for Particle Simulation, a Monte Carlo Simulation Tool for Physics, Biology and Clinical Research.," *Physica Medica,* vol. 72, pp. 114-121, 2020.

[21] J. Baró, J. Sempau, J. Fernández-Varea and F. Salvat, "PENELOPE: An algorithm for Monte Carlo simulation of the penetration and energy loss of electrons and positrons in matter," *Nuclear Instruments and Methods in Physics Research Section B: Beam Interactions with Materials and Atoms,* vol. 1, pp. 31-46, 1995.

[22] GEANT4 Standard and Low Energy EM Physics working groups, "Lecture 5: GEANT4 Low Energy Electromagnetic Physics," 25-26 October 2011. [Online]. Available: http://geant4.in2p3.fr/IMG/pdf_Lecture-LowEnergyEMPhysics.pdf. [Accessed 25 May 2023].

[23] CERN, "Penelope low-energy electromagnetic models," 18 June 2015. [Online]. Available: https://twiki.cern.ch/twiki/bin/genpdf/Geant4/LowePenelope. [Accessed 25 May 2023].

[24] L. Pandola, C. Andenna and B. Caccia, "Validation of the GEANT4 simulation of bremsstrahlung from thick targets below 3 Me," *Nuclear Instruments and Methods in Physics Research B 350,* pp. 41-48, 2015.

[25] P. Andreo, D. T. Burns and F. Salvat, "On the uncertainties of photon mass energy-absorption coefficients and their ratios for radiation dosimetry," *Pysics in Medicine & Biology,* vol. 57, pp. 2117-2136, 2012.

[26] C. Valdes-Cortez, I. Mansour, M. J. Rivard, F. Ballester, E. Mainegra-Hing, R. M. Thomson and J. Vijande, "A study of Type B uncertainties associated with the photoelectric effect in low-energy Monte Carlo simulations," *Physics in Medicine and Biology,* vol. 66, p. 105014, 2021.

[27] Vlaams Supercomputer Centrum, "Genius hardware," 2024. [Online]. Available: https://docs.vscentrum.be/leuven/tier2_hardware/genius_hardware.html. [Accessed 1 April 2024].

[28] TOPAS MC Inc., "Default Parameters - Materials (Revision 76e0be2f)," 2022. [Online]. Available: https://topas.readthedocs.io/en/latest/parameters/defaults.html#parameters-default-materials. [Accessed 1 April 2024].

[29] GEANT4, "GEANT4 Material Database - NIST Compounds," 15 July 2016. [Online]. Available: https://www.fe.infn.it/u/paterno/Geant4_tutorial/slides_further/Geometry/G4_Nist_Materials.pdf. [Accessed 1 April 2024].

[30] F. Verhaegen, A. Nahum, S. Van de Putte and Y. Namito, "Monte Carlo modelling of radiotherapy kV x-

ray units," *Physics in Medicine and Biology,* vol. 44, pp. 1767-1789, 1999.

[31] J. Hubbell and S. Seltzer, "Tables of X-Ray Mass Attenuation Coefficients and Mass Energy-Absorption Coefficients from 1 keV to 20 MeV for Elements Z = 1 to 92 and 48 Additional Substances of Dosimetric Interest," *NIST Standard Reference Database 126,* 2004.

[32] J. B. Kortright and A. C. Thompson, "X-Ray Data Booklet Section 1.2 X-Ray Emissioin Energies," 2000. [Online]. Available: https://xdb.lbl.gov/Section1/Table_1-2.pdf. [Accessed 1 December 2023].

[33] Netherlands commission on Radiation Dosimetry - Task Group Uniformity Dosimetry Protocols, "Dosimety of low and medium energy X-rays," Netherlands commission on Radiation Dosimetry , s.l., 1997.